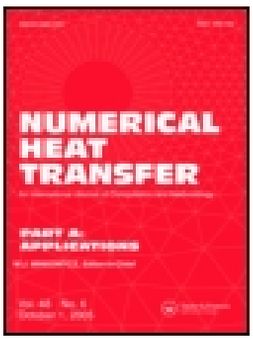

Numerical Heat Transfer, Part A: Applications

ISSN: 1040-7782 (Print) 1521-0634 (Online) Journal homepage: https://www.tandfonline.com/loi/unht20

The Influence of Baffles on the Natural Convection in Trapezoidal Cavities

Éliton Fontana , Adriano da Silva , Viviana Cocco Mariani & Francisco Marcondes

To cite this article: Éliton Fontana , Adriano da Silva , Viviana Cocco Mariani & Francisco Marcondes (2010) The Influence of Baffles on the Natural Convection in Trapezoidal Cavities, Numerical Heat Transfer, Part A: Applications, 58:2, 125-145, DOI: 10.1080/10407782.2010.496673

To link to this article: https://doi.org/10.1080/10407782.2010.496673

Numerical Heat Transfer, Part A, 58: 125–145, 2010

ISSN: 1040-7782 print/1521-0634 online
DOI: 10.1080/10407782.2010.496673

Taylor & Francis
Taylor & Francis Group

THE INFLUENCE OF BAFFLES ON THE NATURAL CONVECTION IN TRAPEZOIDAL CAVITIES

Éliton Fontana[1], Adriano da Silva[2], Viviana Cocco Mariani[3], and Francisco Marcondes[4]

[1]*Universidade Comunitária Regional de Chapecó—UNOCHAPECÓ, Chapecó, Brazil*

[2]*Universidade Federal de São João Del Rei—UFSJ, Divinópolis, Brazil*

[3]*Programa de Pós-Graduação em Engenharia Mecânica— PUCPR, Curitiba, Brazil*

[4]*Departamento de Engenharia Metalúrgica e de Materiais—UFC, Fortaleza, Brazil*

This article presents an investigation into natural convection in trapezoidal cavities. It examines a cavity whose floor and upper inclined walls are both adiabatic, while the vertical walls are isothermal. For these isothermal walls, we consider two thermal boundary conditions. Under the first condition, the short wall on the left side is heated as the tall one on the right side is cooled. The second condition is the reverse of the first—the short wall is cooled as the tall one is heated. Considering laminar conditions and a two-dimensional system, steady-state computations are carried out to assess the effects of one and two baffles, the baffle's height (H_b), Rayleigh number, $10^3 \leq \mathbf{Ra} \leq 10^6$, and three Prandtl number values. To demonstrate the various effects, the results from several designed case studies are shown in terms of isotherms, streamlines, and local and average Nusselt numbers in order. Predictions reveal that the second baffle decreases the cavity's fluid flow and heat transfer. As the height of the baffle rises, the heat transfer drops drastically. Also, two baffles produce more pronounced thermal stratification than only one.

1. INTRODUCTION

Natural convection as an area of study stretches across many fields of science and technology. Disciplines that apply its principles include such a variety as food processing and storage, building insulation, electrochemistry, fire control, metallurgy, meteorology, geophysics, and nuclear reactor systems. This widespread interest in natural convection is underscored in the literature, where intensive investigation is evident. Convection's early investigations, according to Ostrach [1] and Yang [2], focused on heat transfer in simple geometrical cavities—rectangular [3–15]. Studying these simple shapes was necessary because of convection's many thermofluid features, such as recirculation and stagnation regions, boundary layers,

Received 5 December 2009; accepted 12 May 2010.

Address correspondence to Viviana Cocco Mariani, Pontifical Catholic University of Parana—PUCPR, Mechanical Engineering Rua Imaculada Conceição, 1155, Prado Velho, 80215-901, Curitiba, PR, Brazil. E-mail: viviana.mariani@pucpr.br

NOMENCLATURE

b	baffle	Ra	Rayleigh number
g	gravity acceleration, m/s^2	T	temperature, K
H	height of trapezoidal cavity, m	T_0	reference temperature, K
H^*	height of the cavity where the baffle is located, m	T_H	hot temperature, K
		T_C	cold temperature, K
H_b	baffle height, m	u	velocity in x direction, m/s
i	interface	v	velocity in y direction, m/s
k_r	ratio between the thermal conductivity of the baffle and the fluid	W_b	baffle thickness, m
		x, y	Cartesian coordinates, m
L	length of trapezoidal cavity, m	α	thermal diffusivity, m^2/s
L_b	baffle locations, m	β	thermal expansion coefficient of air, 1/K
$\hat{n}$	unit vector normal to the baffle-air interface	θ	inclination of the upper wall of the cavity, ^{o}
$\overline{\mathrm{Nu}}$	average Nusselt number		
Nu_y	local Nusselt number	ν	kinematic viscosity, m^2/s
p	pressure, Pa	ρ	fluid density, kg/m^3
Pr	Prandtl number	$\vec{\nabla}$	gradient vector

and jet deflection. Gebhart [3] and Hoogendoorn [4], working with a square cavity, emphasized various aspects of natural convection flows. Researchers have also investigated inclined cavities in relation to gravitational force [5], examined cavities with nonuniform or three-dimensional temperature on the walls [6–9], and observed the effects on convection in enclosures containing partitions or fins [10–12]. Researchers in recent years, have considered how heat transfer in rectangular cavities is affected by introducing obstacles and attaching fins to the walls [13–15].

Having explored natural convection in rectangular domains, researchers shifted their attention to its behavior in triangular shapes [16–25]. For instance, Karyakin et al. [16] and Holtzman et al. [17] described laminar natural convection in isosceles triangular enclosures heated from below and symmetrically cooled from above. Del Campo et al. [18] modeled the natural convection in triangular enclosures in conjunction with a stream function–vorticity formulation for two aspect ratios and Grashof numbers equal to 10^3 and 10^6. Their investigation is based on a symmetric boundary condition for a system heated from below. Numerical analysis in isosceles triangular enclosures are presented in references [19–24] and in right triangular enclosures in [25].

After investigations into square, rectangular, and triangular patterns, researchers began scrutinizing trapezoidal shapes [26–42]. Producing both experimental and numerical results, Iyican et al. [27, 28] investigated natural convection in an inclined trapezoidal cavity. Their cavity is comprised of a cylindrical cold top, parallel to a hot horizontal surface and plane adiabatic sidewalls. Lam et al. [29] reported similar results for a trapezoidal cavity comprising two vertical, adiabatic walls, a hot floor, and an inclined cold top wall. Kuyper and Hoogendoorn [31] investigated how the inclination angle influences the flow. They also looked at how, in trapezoidal enclosures, the Rayleigh number influences the average Nusselt number for laminar natural convection flow.

Researchers in recent years, have considered how heat transfer in cavities is affected by introducing obstacles and attaching fins to the walls. Moukalled and

Acharya [32–34] observed natural convection heat transfer in a trapezoidal cavity with partial dividers attached to the lower horizontal base [32], to the upper inclined surface of the cavity [33], or to both surfaces [34]. Moukalled and Darwish [35] studied natural convection in a partitioned trapezoidal cavity with one baffle attached to the lower horizontal base. They found that heat transfer is decreased by increasing the Prandtl number and height of the baffle. Boussaid et al. [36] investigated heat transfer within a trapezoidal cavity heated at the bottom and cooled at the inclined top. Moukalled and Darwish [37] investigated the natural convection in trapezoidal cavities with the baffle attached to the upper inclined surface. Moukalled and Darwish [38] investigated the natural convection in trapezoidal cavities with two baffles, where one baffle was attached to the upper inclined surface and the other one was attached to the lower horizontal base.

This article, also investigating natural convection in trapezoidal cavities, analyzes the effects of placing one and two baffles on the cavity's plane horizontal surface. The numerical investigation of natural convection heat transfer in trapezoidal cavities that relate more to the subject discussed here, have been investigated in references [32–35, 37–38]. However, the main difference of the results presented here in relation to previous studies refers to the position of the baffles. As mentioned earlier, most works used one baffle attached to the lower horizontal base or to the inclined upper surface. When two baffles were used in the investigations, one baffle was attached to the upper inclined surface and the other was attached to the horizontal surface. In the present investigation, two baffles are attached to the lower horizontal base. Thus, to the best of our knowledge, such a placement has not yet been studied. We analyze in detail how the number and height (H_b) of adiabatic baffles (of finite thickness, $W_b = L/20$), affect heat transfer. We consider a range of Rayleigh numbers ($10^3 \leq \mathrm{Ra} \leq 10^6$), and three Prandtl number values. The upper inclined and lower horizontal walls are insulated. With a constant temperature, the left and right vertical walls are alternately heated and cooled (uniformly). Therefore, the boundary conditions are the same as those used by reference [35], and similar to references [34, 38] two baffles are used but in different positions. The element-based finite-volume method is employed to solve the nonlinear, coupled, partial differential equations for fluid flow and temperature fields. The results are shown in terms of isotherms, streamlines, and local and average Nusselt numbers.

2. PROBLEM FORMULATION

The general schematic configurations of the two-dimensional trapezoidal cavities (with one and two inside baffles) are shown in Figure 1*a*. The coordinates are shown here as well. Figure 1*b* shows the grid distributions of numerical solutions. The vertical walls of the trapezoidal cavity are heated or cooled at constant temperatures T_H and T_C, where $T_H > T_C$. The horizontal and inclined walls remain adiabatic. The width of the cavity (L) is four times the height (H) of the shortest vertical wall. The inclination of the upper wall of the cavity is fixed at 15°. Baffles are placed at three heights ($H_b = H_{b1} = H_{b2} = H^*/3$, $2H^*/3$, and H^*). H^* denotes the height of the cavity where the baffle is located. One baffle thickness ($W_b = L/20$) and two baffle locations ($L_b = L/3$ or $L_b = 2L/3$, $L_{b1} = L/3$ and $L_{b2} = 2L/3$) are considered.

We assume the fluid properties to be constant. The exception is the density in the buoyancy force term, in the y direction, of the momentum equation. We approximate this term using the Boussinesq approximation. The flow field is considered to be steady state, laminar, and two-dimensional. Therefore, the governing equations for the fluid flow and heat transfer are those expressing the conservation of mass, momentum, and energy. In dimensional form, the transport equations are given by

$$\frac{\partial u}{\partial x}+\frac{\partial v}{\partial y}=0 \tag{1}$$

$$\frac{\partial(uu)}{\partial x}+\frac{\partial(vu)}{\partial y}=-\frac{1}{\rho}\frac{\partial p}{\partial x}+\frac{\partial}{\partial x}\left(\nu\frac{\partial u}{\partial x}\right)+\frac{\partial}{\partial y}\left(\nu\frac{\partial u}{\partial y}\right) \tag{2}$$

$$\frac{\partial(uv)}{\partial x}+\frac{\partial(vv)}{\partial y}=-\frac{1}{\rho}\frac{\partial p}{\partial y}+\frac{\partial}{\partial x}\left(\nu\frac{\partial v}{\partial x}\right)+\frac{\partial}{\partial y}\left(\nu\frac{\partial v}{\partial y}\right)+\beta(T_0-T)g \tag{3}$$

$$\frac{\partial(uT)}{\partial x}+\frac{\partial(vT)}{\partial y}=\frac{\partial}{\partial x}\left(\alpha\frac{\partial T}{\partial x}\right)+\frac{\partial}{\partial y}\left(\alpha\frac{\partial T}{\partial y}\right) \tag{4}$$

where u (m/s) is the velocity in x-direction, v (m/s) is the velocity in y-direction, ρ (kg/m^3) is fluid density, ν (m^2/s) is kinematic viscosity, α (m^2/s) is thermal diffusivity ($\alpha = k/\rho c_p$), β (1/K) is the thermal expansion coefficient of air, T_0 (K) is the reference temperature, T (K) is temperature, and g (m/s^2) is gravitational acceleration.

Along the vertical wall, we consider two sets of boundary conditions. In the first, the following Dirichlet conditions are used.

$$T(x=0,y)=T_C \tag{5}$$

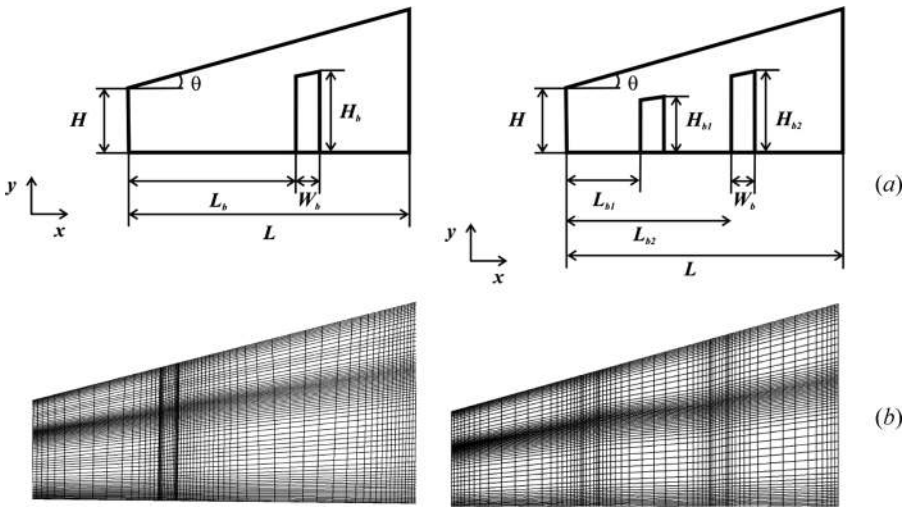

Figure 1. (*a*) Physical model and (*b*) 60×60 meshes used for one and two baffles.

$$T(x = L, y) = T_H \tag{6}$$

In the second, Eqs. (5) and (6) are interchanged. That is, $T\ (x = 0,\ y) = T_H$ and $T\ (x = L,\ y) = T_C$. As shown in Eqs. (7)–(10), we assume no-slip velocities on all walls.

$$u(x = 0, y) = v(x = 0, y) = 0 \tag{7}$$

$$u(x = L, y) = v(x = L, y) = 0 \tag{8}$$

$$u(x, y = 0) = v(x, y = 0) = 0 \tag{9}$$

$$u(x, y = H + xtg(\theta)) = v(x, y = H + xtg(\theta)) = 0 \tag{10}$$

The bottom and top walls remain insulated.

$$\frac{\partial T}{\partial y}\Big)_{y=0} = 0 \tag{11}$$

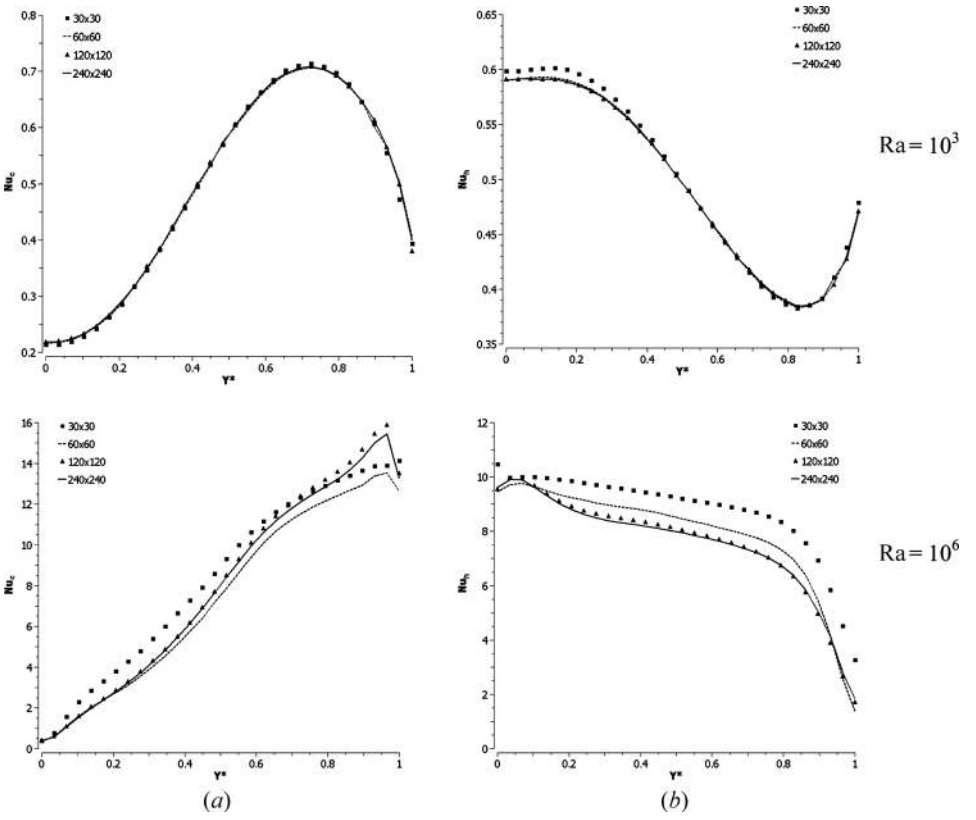

Figure 2. Mesh refinement study: Local Nusselt number for buoyancy-assisting boundary condition, ($H_b = 2H^*/3$, $L_b = L/3$). (*a*) Cold wall and (*b*) hot wall.

$$\left.\frac{\partial T}{\partial y}\right)_{y=H+xtg(\theta)} = 0 \tag{12}$$

The energy balance at the baffle-air interface can be stated as

$$-\frac{1}{\mathrm{Pr}}(\hat{n}.\vec{\nabla}\theta)_i = -\frac{k_r}{\mathrm{Pr}}(\hat{n}.\vec{\nabla}\theta_b)_i \tag{13}$$

where $\hat{n}$ is a unit vector normal to the baffle-air interface, the subscript i refers to the interface, and k_r is the ratio between the thermal conductivity of the baffle and the fluid. The Rayleigh number, for all results shown, is based on the shortest length of the vertical wall. Therefore, the Rayleigh number is defined by

$$\mathrm{Ra} = g\beta(T_H - T_C)H^3/\nu\alpha \tag{14}$$

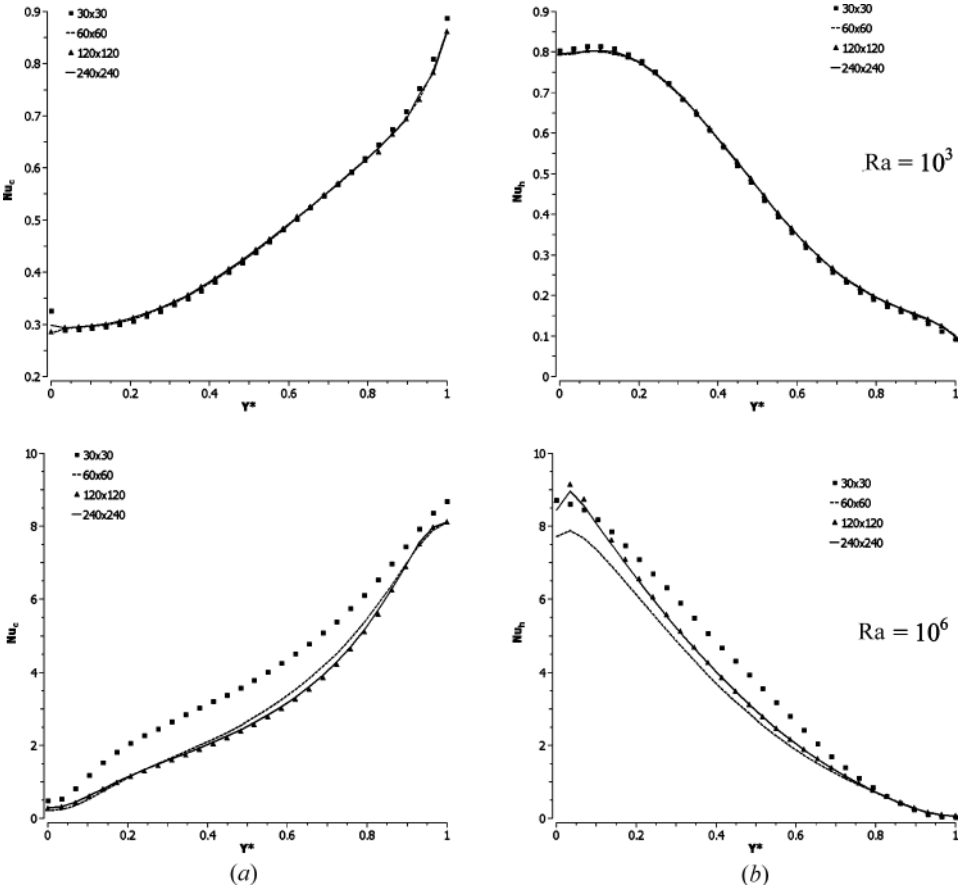

Figure 3. Mesh refinement study: Local Nusselt number for buoyancy-opposing boundary condition, ($H_b = 2H^*/3$, $L_b = L/3$). (*a*) Cold wall and (*b*) hot wall.

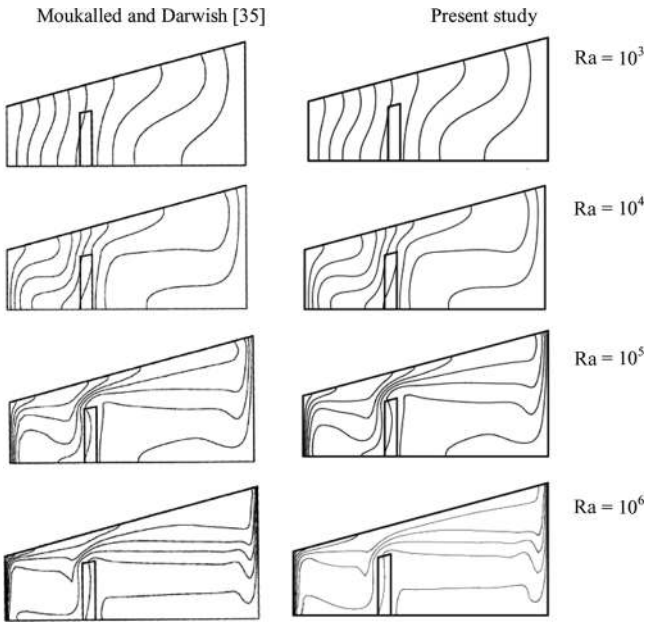

Figure 4. Isotherms ($H_b = 2H^*/3$, $L_b = L/3$) for the buoyancy-assisting boundary condition.

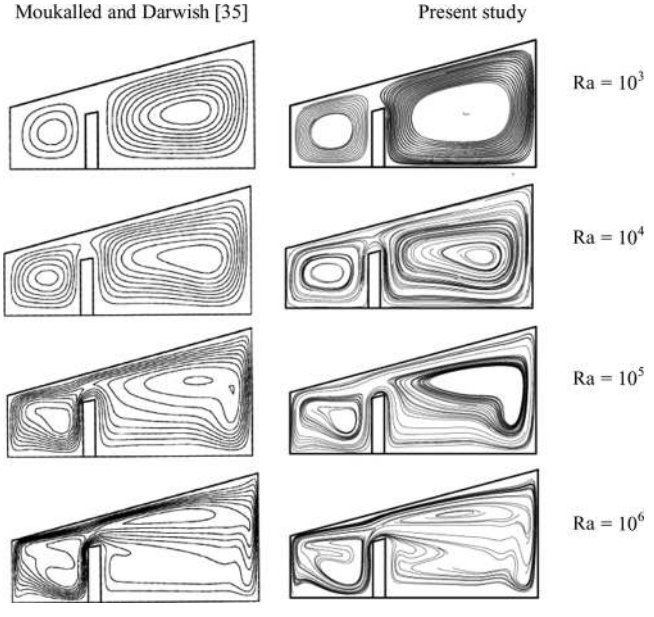

Figure 5. Streamlines ($H_b = 2H^*/3$, $L_b = L/3$) for the buoyancy-assisting boundary condition.

3. NUMERICAL METHODOLOGY

We solve the governing equations using the commercial computational fluid dynamics code ANSYS CFX version 11.0 [43]. In this code, the conservation equations for mass and momentum are solved together using an element-based finite-volume method (EbFVM). The resulting discrete system of linear equations

Table 1. Average Nusselt numbers ($\overline{\mathrm{Nu}}$) for the buoyancy-opposing boundary condition along the cold left and hot right walls for $\mathrm{Pr}=0.7$ and $L_b=L/3$

	Moukalled and Darwish [35]			Present study		
Ra	$H_b=H^*/3$	$H_b=2H^*/3$	$H_b=0$	$H_b=H^*/3$	$H_b=2H^*/3$	$H_b=0$
10^3	0.5080	0.4790	0.6153	0.5030	0.4829	0.6175
10^4	1.4750	0.9880	1.9220	1.4517	1.0140	1.9223
10^5	3.6780	2.1456	4.4310	3.4042	2.3144	4.3409

Table 2. Average Nusselt numbers ($\overline{\mathrm{Nu}}$) for the buoyancy-opposing boundary condition along the cold left and hot right walls for $\mathrm{Pr}=0.7$ and $L_b=2L/3$

	Moukalled and Darwish [35]			Present study		
Ra	$H_b=H^*/3$	$H_b=2H^*/3$	$H_b=0$	$H_b=H^*/3$	$H_b=2H^*/3$	$H_b=0$
10^3	0.5040	0.4640	0.6153	0.5037	0.4710	0.6175
10^4	1.5510	1.0720	1.9220	1.5619	1.1080	1.9223
10^5	3.5640	2.2940	4.4310	3.6236	2.4361	4.3409

Table 3. Average Nusselt numbers ($\overline{\mathrm{Nu}}$) for buoyancy-assisting boundary condition along the cold right and hot left walls for $\mathrm{Pr}=0.7$ and $L_b=2L/3$

	Moukalled and Darwish [35]			Present study		
Ra	$H_b=H^*/3$	$H_b=2H^*/3$	$H_b=0$	$H_b=H^*/3$	$H_b=2H^*/3$	$H_b=0$
10^3	0.5670	0.4900	0.7150	0.5676	0.4976	0.7167
10^4	2.2560	1.3050	2.4800	2.2801	1.3127	2.5068
10^5	5.1660	3.9450	5.4760	5.3670	4.0084	5.6942

Table 4. Average Nusselt numbers ($\overline{\mathrm{Nu}}$) for buoyancy-assisting boundary condition along the cold right and hot left walls for $\mathrm{Pr}=0.7$ and $L_b=L/3$

	Moukalled and Darwish [35]			Present study		
Ra	$H_b=H^*/3$	$H_b=2H^*/3$	$H_b=0$	$H_b=H^*/3$	$H_b=2H^*/3$	$H_b=0$
10^3	0.5460	0.5030	0.7150	0.5368	0.5033	0.7167
10^4	2.1420	1.1310	2.4800	2.1324	1.1542	2.5068
10^5	5.3030	3.5570	5.4760	5.4902	3.8112	5.6942

is solved using an algebraic multigrid methodology called the additive correction multigrid method. The solution was considered converged when the sum of absolute normalized residuals for all cells in the domain solution was less than 10^{-6}.

4. NUMERICAL RESULTS

This section, which presents the results for several cavity configurations and Rayleigh numbers, is divided into three parts. First, is the mesh refinement study; second, is the numerical validation; and third, are the results for configurations with two baffles.

4.1. Mesh Refinement Study

A mesh refinement was performed for all cavities and Rayleigh numbers investigated. The analysis was based on the local and average Nusselt numbers along

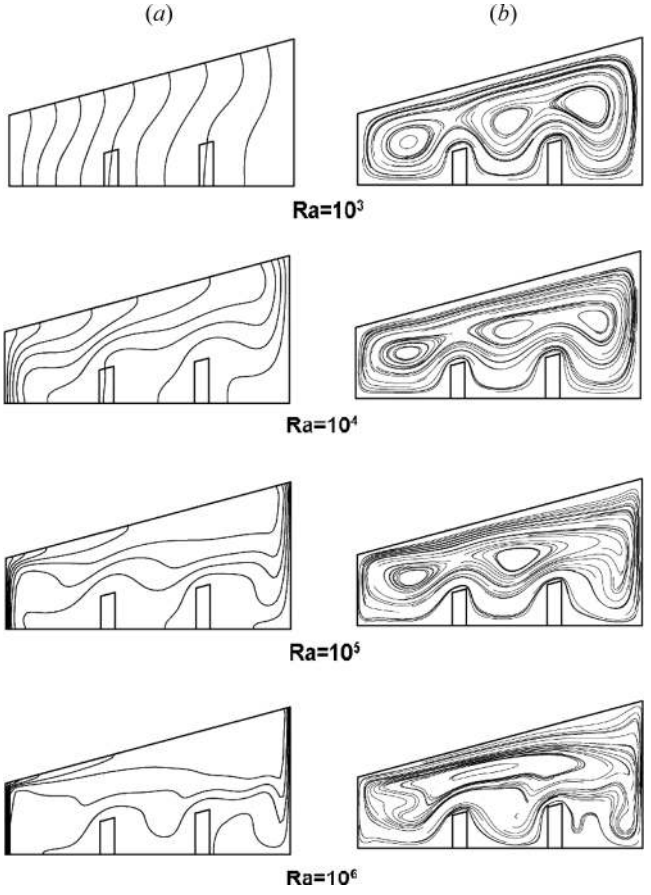

Figure 6. (*a*) Isotherms, and (*b*) streamlines for the buoyancy-assisting boundary condition ($H_{b1} = H_{b2} = H^*/3$, $L_{b1} = L/3$, and $L_{b2} = 2L/3$).

the hot or cold walls, which were defined by

$$\mathrm{Nu}_y = -\partial T/\partial x)_{x=0,x=L}/(T_H - T_c) \tag{15}$$

$$\overline{\mathrm{Nu}} = \frac{1}{H^*}\int_0^L \mathrm{Nu}_y \, dy \tag{16}$$

where H^* denotes the height of either the hot or cold wall. Based on this definition, the average Nusselt numbers along both walls hot and, cold must be the same.

The refinement was mainly promoted at the walls of the trapezoidal cavity and next to the baffle(s), where the gradients are expected to be higher. Four different nonuniform grids composed of 30×30, 60×60, 120×120, and 240×240 grids were used. Figures 2 and 3 present some local Nusselt numbers that were obtained. These are for the buoyancy-assisting boundary condition (left hot wall) and buoyancy opposing boundary condition (right hot wall), respectively, for Ra equal to 10^3

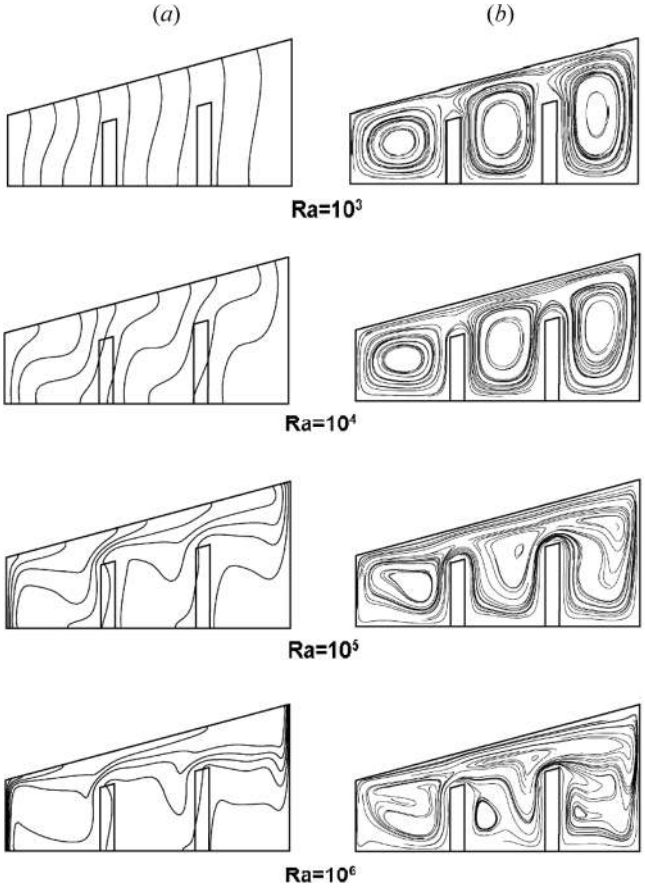

Figure 7. (*a*) Isotherms, and (*b*) streamlines for the buoyancy-assisting boundary condition ($H_{b1} = H_{b2} = 2H^*/3$, $L_{b1} = L/3$, and $L_{b2} = 2L/3$).

and 10^6. The curves for the other investigated configurations are not shown, though curves similar to those presented in Figures 2 and 3 were obtained. Since the differences between the results obtained with 60×60, 120×120, and 240×240 grids were minor, we chose to use the 60×60 nonuniform grid for all simulations presented in this work.

4.2. Numerical Validation for One Baffle

To validate the numerical solution of the present work, some solutions obtained from a trapezoidal cavity with one baffle inside have been compared with results obtained by Moukalled and Darwish [35]. Figures 4 and 5 present the isotherms and streamlines, and Tables 1–4, the average Nusselt number for $L_b = L/3$, $H_b = 2H^*/3$, and $\mathrm{Pr} = 0.7$.

We can see in Figure 4, that for low Rayleigh, the temperature varies almost linearly inside the cavity, indicating that conduction is a dominant heat transfer

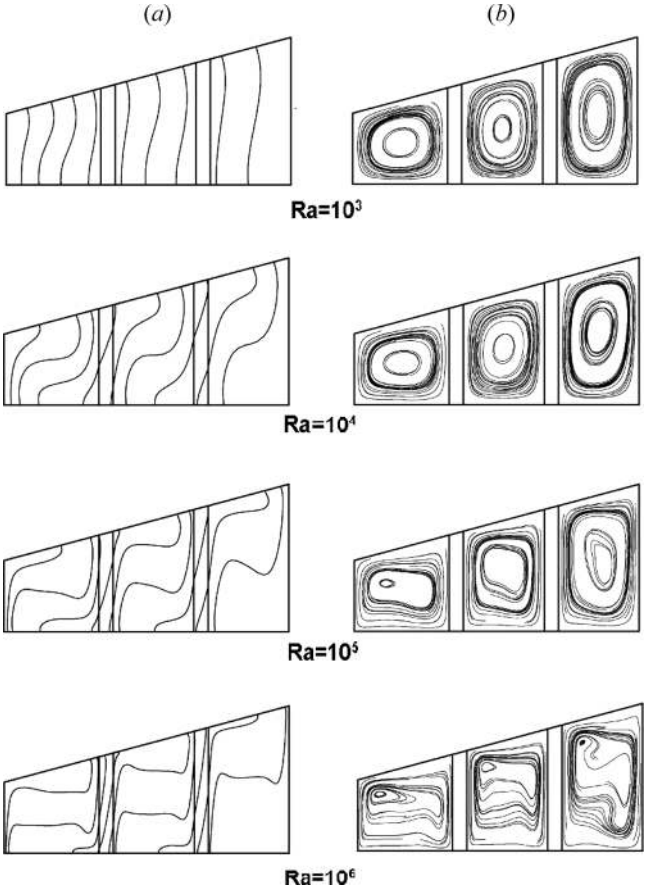

Figure 8. (*a*) Isotherms, and (*b*) streamlines for the buoyancy-assisting boundary condition ($H_{b1} = H_{b2} = H^*$, $L_{b1} = L/3$, and $L_{b2} = 2L/3$).

mode. As the Rayleigh number increases, convection picks up, and isotherms become more distorted. Streamlines in Figure 5 indicate that for the lowest Rayleigh number presented, $\mathrm{Ra} = 10^3$, the recirculation flow exhibits two vortices communicating through a very thin overall rotating eddy (Figure 5*a*). These two vortices rotate clockwise. As the Rayleigh number increases, communication between the vortices increases until the two vortices merge into one at $\mathrm{Ra} = 10^5$ (Figure 5*c*). Moreover, at higher Rayleigh numbers, the flow between the baffle and the cold wall weakens compared to that between the baffle and the hot wall. Despite the weak flow in the lower right-hand portion of the domain, the stratification effects are not strong enough to cause separation. We emphasize the good agreement between these results with one baffle and those obtained by Moukalled and Darwish [35]. Also showing good agreement with their findings, are the average Nusselt numbers (Tables 1–4) for buoyancy-assisting and opposing modes.

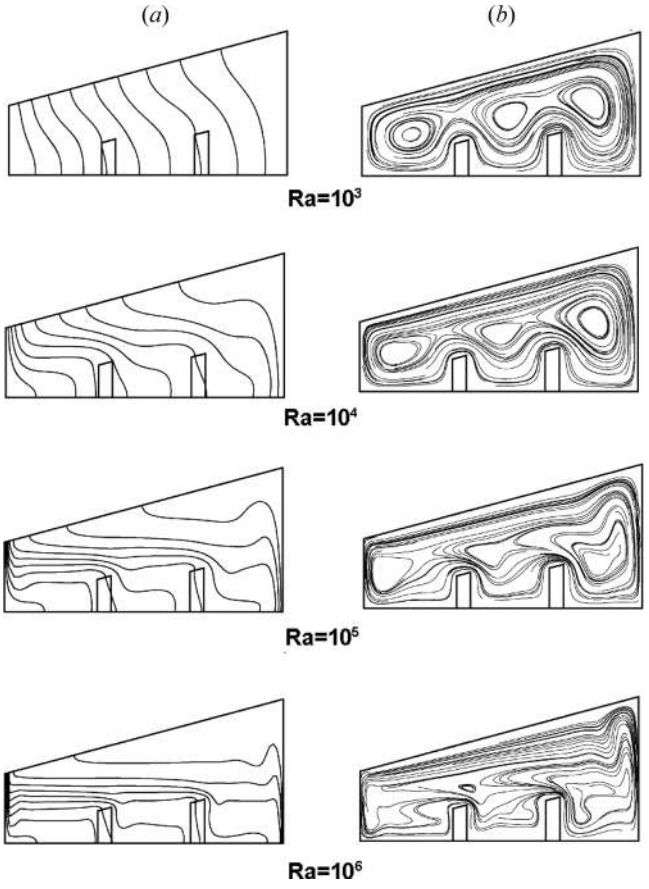

Figure 9. (*a*) Isotherms, and (*b*) streamlines for the buoyancy-opposing boundary condition ($H_{b1} = H_{b2} = H^*/3$, $L_{b1} = L/3$, and $L_{b2} = 2L/3$).

4.3. Results for Two Baffles

Figures 6–8 present the isotherms and streamlines for buoyancy-assisting boundary condition for the Rayleigh numbers in the range $10^3 \leq \mathrm{Ra} \leq 10^6$. Figure 6 reveals a flow caused by the second baffle, composed of a low velocity single counterclockwise rotation cell. It possesses internal single cells between the baffles and vertical walls. For $\mathrm{Ra} = 10^5$, two vortices, the one between the two baffles and the other close to the cold wall, merged. Further increasing the Rayleigh number joins the three internal vortices into a single cell. The isotherms for low Ra are similar to the natural convection with just one baffle. When Ra is increased, however, a thermal stratification close the lower and inclined wall of the cavity is observed. Figures 7 and 8 show the isotherms and streamlines for the two other heights of the baffles. For small Ra, similar streamlines and isotherms to the ones presented in Figure 6 were obtained. For large Ra, a more stratified temperature field is observed and secondary vortices in the region between the baffles appear, as they also do close to the cold wall. The flow is

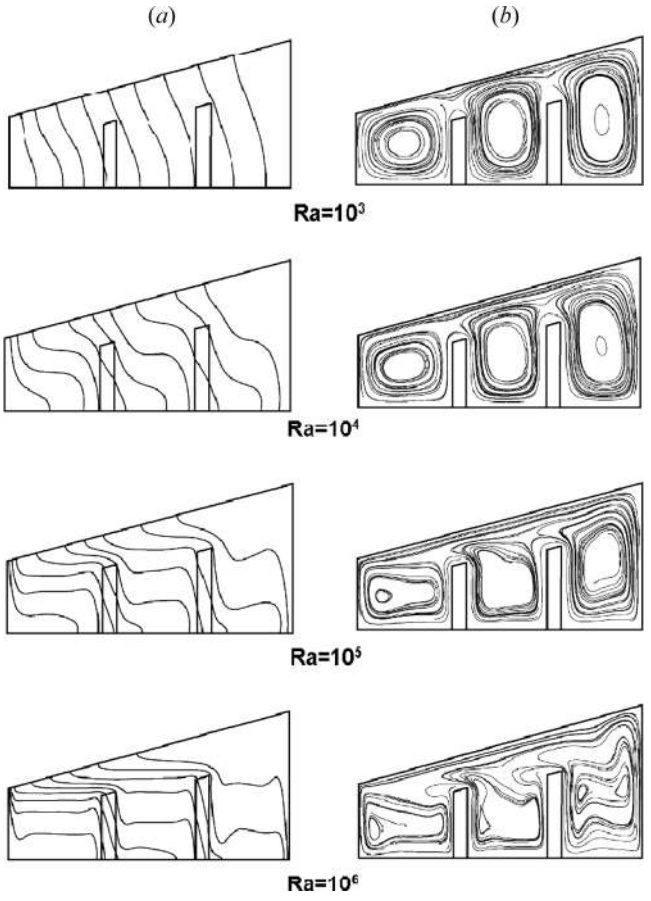

Figure 10. (*a*) Isotherms, and (*b*) streamlines for the buoyancy-opposing boundary condition ($H_{b1} = H_{b2} = 2H^*/3$, $L_{b1} = L/3$, and $L_{b2} = 2L/3$).

more intensive in the region close to the heated wall. Figure 8 reveals a pattern of isotherms and streamlines similar to those seen in Figure 7. What is different, are the resistances to the flow and heat transfer now amplified by the baffles that divide the cavity into three subcavities. The increase in the resistances decreases the thermal and velocity gradients. The isotherms presented in Figure 8 clearly show this behavior.

Figures 9–11 show the isotherms and streamlines, for buoyancy-opposing boundary condition for Rayleigh numbers in the range $10^3 \leq \mathrm{Ra} \leq 10^6$. Again, for small Ra, we observed a behavior, in terms of streamlines and isotherms, similar to that obtained under the buoyancy-assisting boundary condition. Compared to the buoyancy-assisting boundary condition, however, the stratification increases for the same height of baffle and Ra. The thermal stratification increases along the inclined and lower wall of the cavity. Consequently, the pattern of streamlines and isotherms differs completely at high Ra numbers from that found under the buoyancy-assisting boundary condition. The increase of thermal stratification might still reduce the heat transfer inside the cavity.

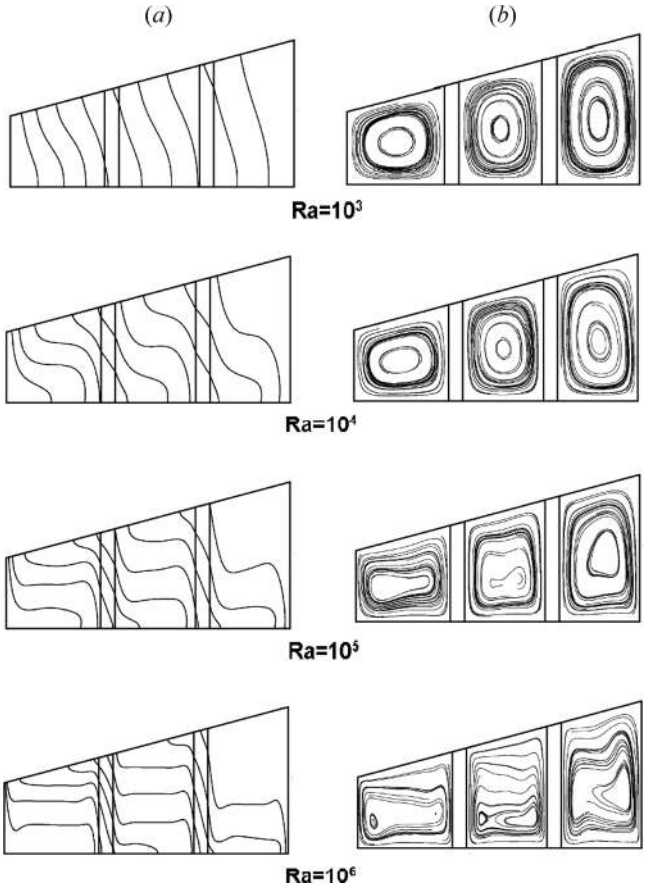

Figure 11. (*a*) Isotherms, and (*b*) streamlines for the buoyancy-opposing boundary condition ($H_{b1} = H_{b2} = H^*$, $L_{b1} = L/3$, and $L_{b2} = 2L/3$).

4.4. Local and Average Heat Transfer Distribution for Two Baffles

This section provides the local and average Nusselt numbers for the two investigated boundary conditions. This data helps quantify the effect of the baffles' height and the Rayleigh number on the natural convection inside the cavity. Figures 12–14 present the local Nusselt numbers for the assisting-boundary condition for the baffles' three heights ($H^*/3$, $2H^*/3$, and H^*). In these figures, Y^* denotes the dimensionless height of the cold or hot wall. Note, that as the height of the baffle increased, the heat transfer drastically decreased. We discussed the reasons for this behavior when presenting the patterns of the isotherms and streamlines. Moreover, for small Ra numbers conduction dominates the heat transfer. This is evidenced for all cases with $\mathrm{Ra} = 10^3$ by the constant local Nusselt number along both vertical walls. We can see that for all cases, the highest value of local Nusselt number is found close to the lower section of the hot wall and close to the upper section of the cold wall. Also, for each Ra value, the highest value of the local Nusselt number is attained in the cold wall. We explain this by pointing out the highest thermal stratification occurs in the lower section of the cold wall. This means that there is less space for the fluid coming from the upper inclined wall of the cavity to exchange energy in the cold vertical wall of the cavity. Then, the gradients between that fluid and the lower section of the hot wall will be smaller compared to the fluid coming from the hot wall, and going straight to the upper section of the cold wall. For trapezoidal cavities with one baffle, Moukalled and Darwish [35] obtained similar results.

Figures 15–17 present the local Nusselt numbers for the buoyancy-opposing boundary condition for baffles at three heights ($H^*/3$, $2H^*/3$, and H^*). The findings here are the same as those for the buoyancy-assisting boundary condition discussed above. More importantly, for each investigated configuration and Ra value, the local Nusselt values are smaller than the case with two baffles under the buoyancy-assisting boundary condition. We explain such behavior as follows. Under the

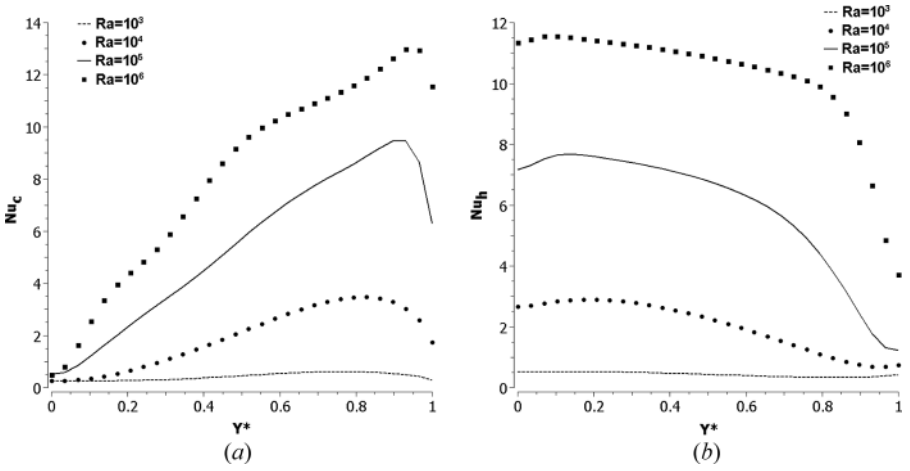

Figure 12. Local Nusselt number for the buoyancy-assisting boundary condition ($H_{b1} = H_{b2} = H^*/3$, $L_{b1} = L/3$, and $L_{b2} = 2L/3$). (*a*) Cold wall and (*b*) hot wall.

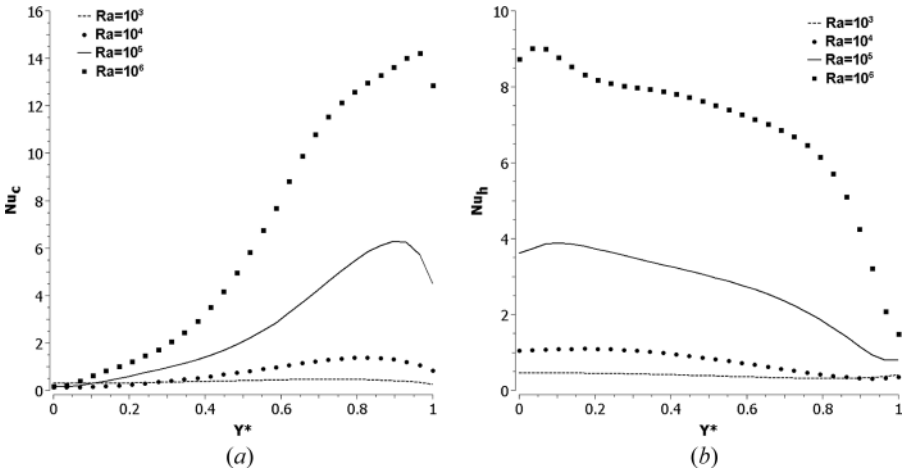

Figure 13. Local Nusselt number for the buoyancy-assisting boundary condition ($H_{b1} = H_{b2} = 2H^*/3$, $L_{b1} = L/3$, and $L_{b2} = 2L/3$). (*a*) Cold wall and (*b*) hot wall.

opposing boundary condition, the fluid has less space to exchange energy along the vertical walls of the cavity, thus decreasing the heat transfer. Moukalled and Darwish [35] reported the same behavior for trapezoidal cavities with one baffle. Table 5 shows the average Nusselt number along the hot wall for assisting and opposing boundary conditions. Similar to Moukalled and Darwish's findings [35], it was verified that for trapezoidal cavities with one baffle a large decrease in the heat transfer when the height of the baffle was increased from $H^*/3$ to $2H^*/3$. When the baffle height was equal to H^*, conduction mode nearly dominates the heat transfer and for all investigated Ra numbers the average Nusselt number varied only slightly.

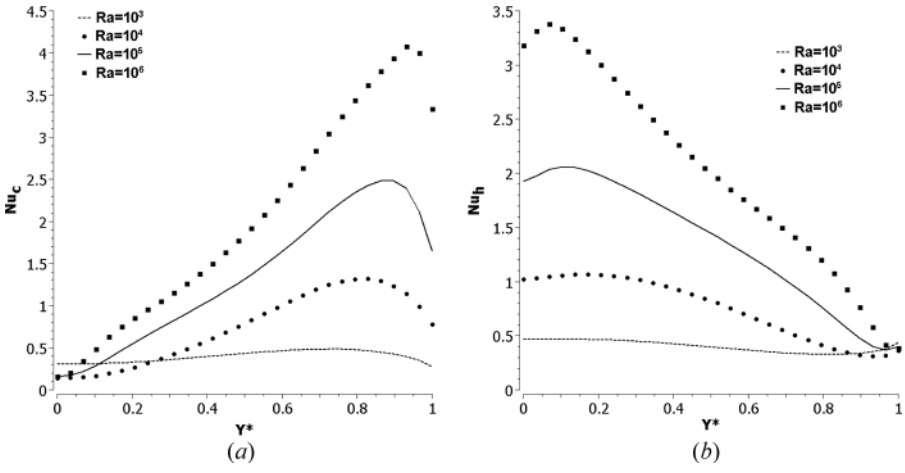

Figure 14. Local Nusselt number for the buoyancy-assisting boundary condition ($H_{b1} = H_{b2} = H^*$, $L_{b1} = L/3$, and $L_{b2} = 2L/3$). (*a*) Cold wall and (*b*) hot wall.

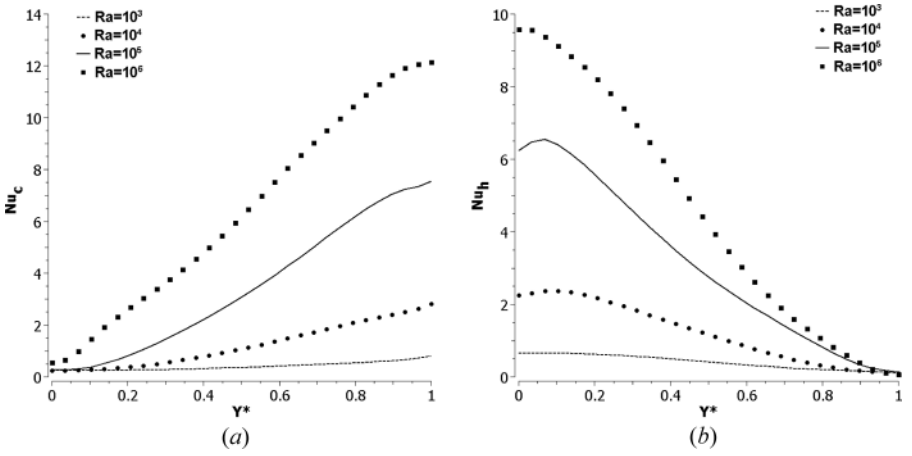

Figure 15. Local Nusselt number for the buoyancy-opposing boundary condition ($H_{b1} = H_{b2} = H^*/3$, $L_{b1} = L/3$, and $L_{b2} = 2L/3$). (*a*) Cold wall and (*b*) hot wall.

From Table 5, it is also possible to verify that the results for two baffles are close to the ones presented for two offset baffles by Moukalled and Darwish [34] when the baffle height was equal to H^*.

The average Nusselt number values for a cavity with the left vertical wall heated and the right vertical wall cooled, was investigated here for three Prandtl numbers (0.7, 10, and 130);, such results are listed in Table 6, respectively. As previously discussed, it is possible to observe from the table that for a fixed Prandtl and Rayleigh number a significant reduction in heat transfer occurs when the baffle height is increased. For the smallest Rayleigh number, the average Nusselt number tends to a constant value when the baffle height is increased. For a given baffle height,

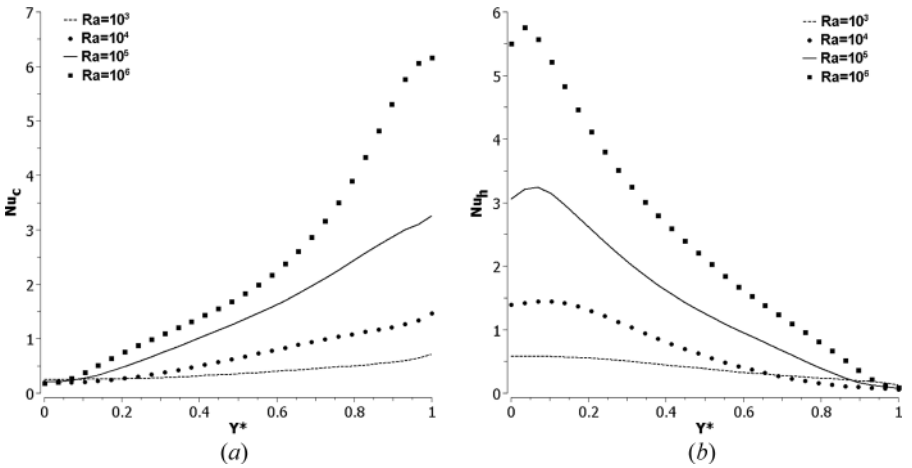

Figure 16. Local Nusselt number for the buoyancy-opposing boundary condition ($H_{b1} = H_{b2} = 2H^*/3$, $L_{b1} = L/3$, and $L_{b2} = 2L/3$). (*a*) Cold wall and (*b*) hot wall.

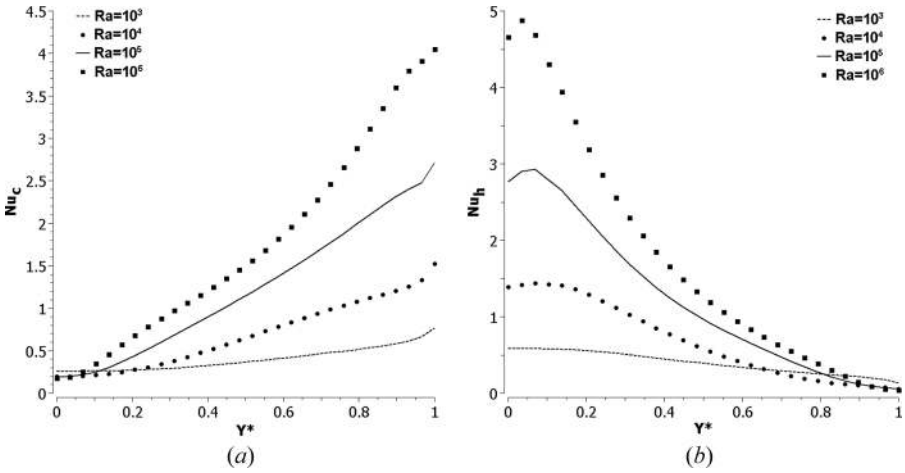

Figure 17. Local Nusselt number for the buoyancy-opposing boundary condition ($H_{b1} = H_{b2} = H^*$, $L_{b1} = L/3$, and $L_{b2} = 2L/3$). (*a*) Cold wall and (*b*) hot wall.

the total heat transfer increases with increasing Ra values due to an increase in convection heat transfer. The average Nusselt number increases with increasing Pr due to a decrease in the thermal boundary layer thickness along the walls with a consequent increase in the temperature gradient close to the hot and cold walls. Note, that the rate of heat transfer increases with increasing Rayleigh and Prandtl numbers.

Table 5. Average Nusselt number values ($\overline{\mathrm{Nu}}$) along the hot wall for buoyancy-assisting and opposing boundary condition and $\mathrm{Pr} = 0.7$

	Buoyancy-assisting			Buoyancy-opposing		
Ra	$H_b = H^*/3$	$H_b = 2H^*/3$	$H_b = H^*$	$H_b = H^*/3$	$H_b = 2H^*/3$	$H_b = H^*$
10^3	0.4456	0.3995	0.40489	0.4228	0.393667	0.4039
10^4	1.9760	0.7826	0.7519	1.2433	0.703451	0.6958
10^5	5.2650	2.7623	1.3501	3.3088	1.48521	1.2428
10^6	8.2412	7.0313	2.0288	6.2760	2.74018	1.9856

Table 6. Average Nusselt number values ($\overline{\mathrm{Nu}}$) along the hot wall for buoyancy-assisting boundary condition for $\mathrm{Pr} = 0.7$, 10, and 130

	$H^*/3$	$2H^*/3$	H^*	$H^*/3$	$2H^*/3$	H^*	$H^*/3$	$2H^*/3$	H^*
	$\mathrm{Pr} = 0.7$			$\mathrm{Pr} = 10$			$\mathrm{Pr} = 130$		
$\mathrm{Ra} = 10^3$	0.4456	0.3995	0.4049	0.4531	0.4001	0.4056	0.4528	0.4003	0.4056
$\mathrm{Ra} = 10^4$	1.9760	0.7826	0.7519	2.1385	0.8038	0.7646	2.1388	0.8040	0.7646
$\mathrm{Ra} = 10^5$	5.2650	2.7623	1.3501	6.3202	3.3376	1.4087	6.3199	3.3481	1.4092
$\mathrm{Ra} = 10^6$	8.2412	7.0313	2.0288	9.9527	8.7489	2.4207	9.9542	8.9081	2.4221

5. CONCLUSION

We have presented an investigation into natural convection in partitioned trapezoidal cavities with one and two internal baffles. The conservation equations in terms of the primitive variables were solved by the finite-volume method. This work investigated several physical parameters, including the number of baffles, boundary conditions (buoyancy-assisting and buoyancy-opposing modes), and position of the baffles. We presented our results in terms of isotherms, streamlines, and local and average Nusselt number. We observed that the second baffle decreased the cavity's fluid flow and heat transfer. As the height of the baffle rose, the heat transfer dropped drastically. Also, when there were two baffles, thermal stratification was much more pronounced than when there was only one.

REFERENCES

1. S. Ostrach, Natural Convection in Enclosures, *J. Heat Transfer*, vol. 110, pp. 1175–1190, 1988.
2. K. T. Yang, Transitions and Bifurcations in Laminar Buoyant Flows in Confined Enclosures, *J. Heat Transfer*, vol. 110, pp. 1191–1204, 1988.
3. B. Gebhart, Buoyancy-Induced Fluid Motions Characteristics of Applications in Technology: The 1978 Freeman Scholar Lecture, *ASME J. Fluids Eng.*, vol. 101, pp. 5–28, 1979.
4. C. J. Hoogendoorn, Natural Convection in Enclosures, Proc. of 8th International Heat Transfer Conf., vol. I, pp. 111–120, Hemisphere Publishing Corporation, San Francisco, 1986.
5. M. A. R. Sharif and W. Liu, Numerical Study of Turbulent Natural Convection in a Side-Heated Square Cavity at Various Angles of Inclination, *Numer. Heat Transfer A*, vol. 43, pp. 693–716, 2003.
6. V. Erenburg, A. Y. Gelfgat, E. Kit, P. Z. Bar-Yoseph, and A. Solan, Multiple States, Stability and Bifurcations of Natural Convection in a Rectangular Cavity with Partially Heated Vertical Walls, *J. Fluid Mech.*, vol. 492, pp. 63–89, 2003.
7. W. H. Leong, K. G. T. Hollands, and A. P. Brunger, Experimental Nusselt Numbers for a Cubical-Cavity Benchmark Problem in Natural Convection, *Int. J. Heat Mass Transfer*, vol. 42, pp. 1979–1989, 1999.
8. S. Wakashima and T. S. Saitoh, Benchmark Solutions for Natural Convection in a Cubic Cavity using the High-Order Time-Space Methods, *Int. J. Heat Mass Transfer*, vol. 47, pp. 853–864, 2004.
9. T. Basak, S. Roy, P. K. Sharma, and I. Pop, Analysis of Mixed Convection Flows Within a Square Cavity with Uniform and NonUniform Heating of Bottom Wall, *Int. J. Thermal Sciences*, vol. 48, pp. 891–912, 2009.
10. N. Yucel and A. H. Ozdem, Natural Convection in Partially Divided Square Enclosures, *Heat Mass Transfer*, vol. 40, pp. 167–175, 2003.
11. F. Ampofo, Turbulent Natural Convection in an Air Filled Partitioned Square Cavity, *Int. J. Heat Fluid Flow*, vol. 25, pp. 103–114, 2004.
12. X. Shi and J. M. Khodadadi, Laminar Natural Convection Heat Transfer in a Differentially Heated Square Cavity Due to a Thin on the Hot Wall, *J. Heat Transfer*, vol. 125, pp. 624–634, 2003.
13. R. L. Frederick, Natural Convection in an Inclined Square Enclosure with a Partition Attached its Cold Wall, *Int. J. Heat Mass Transfer*, vol. 31, pp. 87–94, 1989.

14. A. Nag, A. Sarkar, and V. M. K. Sastri, Natural Convection in a Differentially Heated Square Cavity with a Horizontal Partition Plate on the Hot Wall, *Comput. Methods Appl. Mech. Eng.*, vol. 110, pp. 143–156, 1993.
15. S. H. Tasnim and M. R. Collins, Numerical Analysis of Heat Transfer in a Square Cavity with a Baffle on the Hot Wall, *Int. Commun. Heat Mass Transfer*, vol. 31, pp. 639–650, 2004.
16. Y. E. Karyakin, Y. A. Sokovishin, and O. G. Martynenko, Transient Natural Convection in Triangular Enclosures, *Int. J. Heat Mass Transfer*, vol. 31, pp. 1759–1766, 1988.
17. G. A. Holtzman, R. W. Hill, and K. S. Ball, Laminar Natural Convection in Isosceles Triangular Enclosures Heated from Below and Symmetrically Cooled from Above, *J. Heat Transfer*, vol. 122, pp. 485–491, 2000.
18. E. M. Del Campo, M. Sen, and E. Ramos, Analysis of Laminar Natural Convection in a Triangular Enclosure, *Numer. Heat Transfer, Part A*, vol. 13, pp. 353–372, 1988.
19. E. F. Kent, Numerical Analysis of Laminar Convection in Isosceles Triangular Enclosures, Proc. of the Institution of Mechanical Engineers, Part C, *J. Mechanical Eng. Sci.*, vol. 223, pp. 1157–1169, 2009.
20. E. F. Kent, Numerical Analysis of Laminar Convection in Isosceles Triangular Enclosures for Cold Base and Hot Inclined Walls, *Mech. Research Communications*, vol. 36, pp. 497–508, 2009.
21. H. Asan and L. Namli, Numerical Simulation of Buoyant in a Roof of Triangular Cross-Section under Winter Day Boundary Conditions, *Energy and Buildings*, vol. 33, pp. 753–757, 2001.
22. H. Asan and L. Namli, Laminar Natural Convection in a Pitched Roof of Triangular Cross-Section: Summer Day Boundary Conditions, *Energy and Buildings*, vol. 33, pp. 69–73, 2000.
23. E. H. Ridouane and A. Campo, Effects of Attaching Baffles onto the Inclined Walls of Attic Frames for Purposes of Energy Conservation, *Heat Transfer Eng.*, vol. 28, pp. 103–111, 2007.
24. E. Ridouane, A. Campo, and M. Hasnaoui, Benefits Derivable from Connecting the Bottom and Top Walls of Attic Enclosures with Insulated Vertical Side Walls, *Num. Heat Transfer A*, vol. 49, pp. 175–193, 2006.
25. E. F. Kent, E. Asmaz, and S. Ozerbay, Laminar Natural Convection in Right Triangular Enclosures, *Heat and Mass Transfer*, vol. 44, pp. 187–200, 2007.
26. M. Peric, Natural Convection in Trapezoidal Cavities, *Numer. Heat Transfer A*, vol. 24, pp. 213–219, 1993.
27. L. Iyican, Y. Bayazitoglu, and L. C. Witte, An Analytical Study of Natural Convective Heat Transfer within Trapezoidal Enclosure, *J. Heat Transfer*, vol. 102, pp. 640–647, 1980.
28. L. Iyican, L. C. Witte, and Y. Bayazitoglu, An Experimental Study of Natural Convection in Trapezoidal Enclosures, *J. Heat Transfer*, vol. 102, pp. 648–653, 1980.
29. S. W. Lam, R. Gani, and J. G. Simons, Experimental and Numerical Studies of Natural Convection in Trapezoidal Cavities, *J. Heat Transfer*, vol. 111, pp. 372–377, 1989.
30. T. S. Lee, Numerical Experiments with Fluid Convection in Tilted Nonrectangular Enclosures, *Numer. Heat Transfer A*, vol. 19, pp. 487–499, 1991.
31. R. A. Kuyper and C. J. Hoogendoorn, Laminar Natural Convection Flow in Trapezoidal Enclosures'', *Numer. Heat Transfer A*, vol. 28, pp. 55–67, 1995.
32. F. Moukalled and S. Acharya, Buoyancy-Induced Heat Transfer in Partially Divided Trapezoidal Cavities, *Numer. Heat Transfer A*, vol. 32, pp. 787–810, 1997.
33. F. Moukalled and S. Acharya, Natural Convection in Trapezoidal Cavities with Baffles Mounted on the Upper Inclined Surfaces, *Numer. Heat Transfer A*, vol. 37, pp. 545–565, 2000.

34. F. Moukalled and S. Acharya, Natural Convection in Trapezoidal Cavities with two Offset Baffles, *AIAA J. Thermophysics and Heat Transfer*, vol. 15, pp. 212–218, 2001.
35. F. Moukalled and M. Darwish, Natural Convection in a Partitioned Trapezoidal Cavity Heated from the Side, *Numer. Heat Transfer A*, vol. 43, pp. 543–563, 2003.
36. M. Boussaid, A. Djerrada, and M. Bouhadef, Thermosolutal Transfer within Trapezoidal Cavity, *Numer. Heat Transfer A*, vol. 43, pp. 431–448, 2003.
37. F. Moukalled and M. Darwish, Natural Convection in a Trapezoidal Enclosure Heated from the Side with a Baffle Mounted on its Upper Inclined Surface, *Heat Transfer Eng.*, vol. 25, pp. 80–93, 2004.
38. F. Moukalled and M. Darwish, Buoyancy Induced Heat Transfer in a Trapezoidal Enclosure with Offset Baffles, *Numer. Heat Transfer A*, vol. 52, pp. 337–355, 2007.
39. R. Basak, S. Roy, and A. Singh, Natural Convection Flow Simulation for Various Angles in a Trapezoidal Enclosure with Linearly Heated Side Wall(s), *Int. J. Heat and Mass Transfer*, vol. 52, pp. 4413–4425, 2009.
40. B. Tanmay, S. Roy, and I. Pop, Heat Flow Analysis for Natural Convection within Trapezoidal Enclosures Based on Heatline Concept, *Int. J. Heat and Mass Transfer*, vol. 52, pp. 2471–2483, 2009.
41. E. Natarajan, T. Basak, and S. Roy, Natural Convection Flows in a Trapezoidal Enclosure with Uniform and Non-Uniform Heating of Bottom Wall, *Int. J. Heat and Mass Transfer*, vol. 51, pp. 747–756, 2008.
42. K. Lasfer, M. Bouzaiane, and T. Lili, Numerical Study of Laminar Natural Convection in a Side-Heated Trapezoidal Cavity at Various Inclined Heated Sidewalls, *Heat Transfer Eng.*, vol. 31, pp. 362–373, 2010.
43. User Guide for ANSYS CFX Release 11.0, ANSYS Europe Ltd.